2017

Theoretical and experimental investigation of thermal and oxidation behaviours of a high speed steel work roll during hot rolling

Guanyu Deng
Kyoto University, gdeng@uow.edu.au

Hongtao Zhu
University of Wollongong, hongtao@uow.edu.au

Anh Kiet Tieu
University of Wollongong, ktieu@uow.edu.au

Lihong Su
University of Wollongong, lihongsu@uow.edu.au

Mark H. Reid
University of Wollongong, mreid@uow.edu.au

See next page for additional authors

Publication Details

Deng, G. Y., Zhu, H. T., Tieu, A. K., Su, L. H., Reid, M., Zhang, L., Wei, P. T., Zhao, X., Wang, H., Zhang, J., Li, J. T., Ta, T. D., Zhu, Q., Kong, C. & Wu, Q. (2017). Theoretical and experimental investigation of thermal and oxidation behaviours of a high speed steel work roll during hot rolling. International Journal of Mechanical Sciences, 131-132 811-826.

Theoretical and experimental investigation of thermal and oxidation behaviours of a high speed steel work roll during hot rolling

Abstract
In the present study, thermal behaviours of a HSS work roll in actual service condition during hot rolling have been systematically investigated by an experimentally validated model. Influencing factors including finishing stand number, heat transfer coefficients in different circumferential thermal boundaries and initial work roll body temperature have also been carefully examined on the temperature and thermal stress distributions within the work roll. Based on working temperature range at roll surface from the theoretical analysis, oxidation tests of a HSS work roll material have been conducted. It has been observed that the practical HSS oxide scale is obviously different compared to those developed in laboratory not only because of the complicated oxidation atmosphere in industry, but also influenced by the cyclic mechanical load and thermal stress at the work roll surface.

Disciplines
Engineering | Science and Technology Studies

Publication Details
Deng, G. Y., Zhu, H. T., Tieu, A. K., Su, L. H., Reid, M., Zhang, L., Wei, P. T., Zhao, X., Wang, H., Zhang, J., Li, J. T., Ta, T. D., Zhu, Q., Kong, C. & Wu, Q. (2017). Theoretical and experimental investigation of thermal and oxidation behaviours of a high speed steel work roll during hot rolling. International Journal of Mechanical Sciences, 131-132 811-826.

Authors
Guanyu Deng, Hongtao Zhu, Anh Kiet Tieu, Lihong Su, Mark H. Reid, L C. Zhang, Peitang Wei, Xing Zhao, Hui Wang, Jiangshan Zhang, Jintao Li, Thi D. Ta, Qiang Zhu, Charlie Kong, and Q Wu

Theoretical and experimental investigation of thermal and oxidation behaviours of a high speed steel work roll during hot rolling

G.Y. Deng[1,2], H.T. Zhu[3], A.K. Tieu[3], L.H. Su[3], M. Reid[2], L. Zhang[3], P.T. Wei[4], X. Zhao[3], H. Wang[3], J. Zhang[3], J.T. Li[3], T.D. Ta[3], Q. Zhu[5], C. Kong[5], Q. Wu[6]

[1]Department of Materials Science and Engineering, Kyoto University, Kyoto 606-8501, Japan

[2]Australian Centre for Neutron Scattering, Australian Nuclear Science and Technology Organisation, New South Wales 2232, Australia

[3]School of Mechanical, Materials, Mechatronic and Biomedical Engineering, University of Wollongong, New South Wales 2522, Australia

[4]State Key Laboratory of Mechanical Transmission, Chongqing University, Chongqing, China

[5]Electron Microscope Unit, University of New South Wales, New South Wales 2052, Australia

[6]Baosteel Research Institute, Baoshan Iron & Steel Co., Ltd, Shanghai 201900, China

Abstract:

In the present study, thermal behaviours of a HSS work roll in actual service condition during hot rolling have been systematically investigated by an experimentally validated model. Influencing factors including finishing stand number, heat transfer coefficients in different circumferential thermal boundaries and initial work roll body temperature have also been carefully examined on the temperature and thermal stress distributions within the work roll. Based on working temperature range at roll surface from the theoretical analysis, oxidation tests of a HSS work roll material have been conducted. It has been observed that the practical HSS oxide scale is obviously different compared to those developed in laboratory not only because of the complicated oxidation atmosphere in industry, but also influenced by the cyclical mechanical load and thermal stress at the work roll surface.

Keywords: Hot rolling, manufacturing, work roll, oxidation, stress, surface morphology

1. Introduction

Hot rolling has been an attractive industrial process for a very long time due to its capacity to manufacture finished or semi-finished bulk materials at temperatures above their recrystallization points. During hot rolling, very complicated interactions between elastic deformations of work rolls and back-up rolls, plastic deformation of strips and heat transfer among the hot strip, work roll and surrounding environment exist. The work rolls are

cyclically heated during contact with hot strips (due to conduction of heat from strip, deformation and friction works) and cooled by cooling systems, and the fast temperature variations leads to the development of oxide scale, thermal cracks and fatigue at work roll surface [1-4]. Hence, understanding and improvement of the work roll performances in service have been a very important subject for both engineers and scientists.

Due to very complicated relationship between the working temperature of a work roll during hot rolling and its mechanical, tribological and oxidation properties, it is very critical to understand the detailed temperature evolution in a work roll during its service. Steven et al. [5] have conducted the first on-site industrial experiment to measure the temperature changes in a S.G. cast iron work roll in a roughing stand of a medium-width strip mill. Their measurement for the first time confirmed that the work roll surface temperature could be as high as 500°C during hot rolling. Unfortunately no other industrial experiment has been reported up to now except their study because of very complicated experimental operations and extremely high cost in industry. Even though there are several similar measurements on hot rolling of aluminium alloy were conducted in laboratory [6-8], however, those results were not comparable with the industrial cases because a lot of practical influencing factors were not been able to be considered in laboratory.

Except the experimental tools, computational model is fortunately nowadays a powerful and reliable tool for simulating different thermo-mechanical-metallurgical processes from macro-, micro- to nano-scale size, with quick development of computer skills [9-11]. To date, a large number of investigations have already been successfully conducted on modelling thermal behaviours of work rolls during hot rolling. For example, a very early model was proposed by Patula [12] to study the steady state temperature distribution in a rotating roll subject to surface heat fluxes and convective cooling. Then Troeder and co-authors [13] have studied stress distribution based on assumptions of uniform heat flux and convective cooling in a three-dimensional work roll model. Lai et al. [14] calculated the transient thermal stress of a work roll using coupled thermo-elasticity analytical method. The transient thermal behaviours of work rolls have also been studied by Guo [15] and Hwang et al. [16] using two-dimensional finite element models, and by Lee et al. [17] and Li et al. [18,19] using three-dimensional finite element models, respectively. In Ref. [20], Guerrero and co-authors have developed four different mathematical models to study the work roll temperature field during hot rolling, and Sun et al. [21] have proposed an integrated finite element based model for the prediction of steady-state thermo-mechanical behaviour of the roll-strip system and of roll life. Chang [22] developed an analytical model for the thermal

stress of a work roll within the roll bite region with a semi-infinite-solid approximation. Perez et al. [23] predicted the thermal response of a work roll using a mathematical model considering three different levels: independent cycle of the roll, rolling of a strip-rest, and a whole campaign. Strain-life of a work roll during hot rolling was calculated by Corral et al. [24] by means of a hybrid, analytic-numerical model, and temperatures and thermal stress/strains in the roll under various cooling conditions was predicted by Saha et al. [25] applying a mathematical model. In addition, thermal stress and temperature variations within work rolls in hot strip rolling have also been modelled by Fisher et al. [26], Serajzadehet al. [27,28], Benasciutti et al. [29] and Na et al. [30], respectively. In addition to modelling the temperature and thermal stress variations of work rolls as mentioned in the above literatures, analysis on the geometry of water spray and work roll thermal crown profile has also been done as reported in Refs. [31,32] using finite different method.

Since the end of last century, application of high speed steels (HSS) work rolls during hot rolling in industry has been increased quickly and made a breakthrough due to their excellent wear resistance, hardness, and high temperature service performances [33-35]. It has been reported that the HSS work rolls have about three times longer service life than the high chromium cast iron rolls [36]. As revealed by many experimental and theoretical reports, working temperature at work roll surface during hot rolling could be very high and oxidation of work rolls cannot be avoided. Therefore, accurate understanding the oxidation behaviour of hot rolling work rolls is very crucial and a number of efforts have been contributed on investigating oxidation behaviours of HSS roll materials already. For example, Kim et al. [37] have reported a significant influence of alloy elements vanadium (V) and chromium (Cr) by oxidizing three different HSS materials at 600°C. More details can be found in [38-40], where Cr-rich M_7C_3 carbide had the best oxidation resistance than carbides MC and M_2C because it dissolved high amount of chromium. Those observations were confirmed by the recent studies [41,42] by analyzing the morphology and microstructure evolutions of oxidized HSS samples. Zhou et al. [43,44] have compared the oxidation rate of a HSS material at different temperatures and they have concluded that the matrix was easier than the carbides to be oxidized at low temperatures. However, their conclusions obviously contradict with the results shown in [37-40,45]. In addition, Yin et al. [46] have recently reported that the HSS oxide scale thickness was as large as 5 μm after 2 hours oxidations below 600 °C. Actually, the oxide scale in their study was much thicker compared to the previous reports. Except the above mentioned contradictions, majority of the available reports were conducted in laboratory and the oxidation time was much longer than the

practical work roll contact time (generally less than one hour) during industrial hot rolling. Therefore, systematical investigation on the oxide scale formation mechanism at HSS work roll surface within reasonable short time is still necessary, and particularly comparison with a practical oxide scale has never been reported yet.

For a better understanding of oxidation behavior of a HSS work roll in actual service condition during hot rolling, accurate understanding of temperature evolution in the HSS work roll in actual service condition is extremely important and should come first. However, it has been found that very limited reports on temperature analysis of HSS work rolls were available after a careful literatures review. Only two reports [4,30] have been conducted based on practical industrial steel hot rolling process.

The present study is an extension from our previous work [4], and there are three main objectives. Firstly, systematical theoretical analysis on the temperature and thermal stress evolution in a HSS work roll of an industrial hot strip mill is conducted based on finite element models. Influences of thermal boundary conditions and initial work roll body temperature are discussed in details. Then, oxidation experiment of the HSS work roll material is conducted in working temperature range at a work roll surface during industrial hot rolling provided by the theoretical analysis. Surface morphology of the oxidized HSS samples and cross-sections of those oxide scales are carefully examined with a help of scanning electron microscope (SEM), focused ion beam (FIB) and transmission electron microscope (TEM). Influences of the oxidation atmosphere and temperature have been discussed. Finally, comparisons between an industrial practical oxide scale on a HSS work roll and the laboratory developed oxide scales are made in terms of surface morphology and scale thickness. It should be noted that, the present study is the first report on systematically evaluating the temperature, thermal stress and oxide scale evolutions of a HSS work roll in practical steel hot rolling conditions, and it is an important guidance for the steel makers.

2. Description of theory

2.1 Basic mathematic model

As reported in many literatures [1,4,7,18,19,31,32], heat flows from the hot strip to the work rolls when they contact during hot rolling process because there is a large temperature difference between the strip and work roll surface. The general heat transfer mathematical constitutive law in cylindrical coordinates (r- θ- z) can be written as

$$\left[\frac{1}{r}\frac{\partial}{\partial r}\left(K_w r\frac{\partial T(t)}{\partial r}\right)+\frac{1}{r^2}\frac{\partial}{\partial \theta}\left(K_w\frac{\partial T(t)}{\partial \theta}\right)+\frac{\partial}{\partial z}\left(K_w\frac{\partial T(t)}{\partial z}\right)\right]+\dot{Q}(t)-\left[\rho_w C_w v_r\frac{\partial T(t)}{\partial r}+\rho_w C_w\frac{v_\theta}{r}\frac{\partial T(t)}{\partial \theta}+\rho_w C_w v_z\frac{\partial T(t)}{\partial z}\right]-\rho_w C_w\frac{\partial T(t)}{\partial t}=0 \quad (1)$$

where r, θ, and z are the radial, circumferential and longitudinal directions of the work roll; $T(t)$ is transient temperature; t means time; $\dot{Q}(t)$ means source of energy inside the work roll; K_w, ρ_w and C_w are the thermal conductivity, density, and specific heat of work roll, respectively.

Assuming no source of energy inside the work roll ($\dot{Q}(t)=0$), no movement along the radial direction ($v_r\frac{\partial T(t)}{\partial r}=0$) and longitudinal direction ($v_z\frac{\partial T(t)}{\partial z}=0$), and energy transport along the circumferential direction dominated by convection but not conduction ($\frac{v_\theta}{r}\frac{\partial T(t)}{\partial \theta}=0$), then Eq. (1) can be simplified as Eq. (2) for a transient state thermal condition ($\frac{\partial T(t)}{\partial t}\neq 0$).

$$\frac{1}{r}\frac{\partial}{\partial r}\left(K_w r\frac{\partial T(t)}{\partial r}\right)+\frac{1}{r^2}\frac{\partial}{\partial \theta}\left(K_w\frac{\partial T(t)}{\partial \theta}\right)+\frac{\partial}{\partial z}\left(K_w\frac{\partial T(t)}{\partial z}\right)-\rho_w C_w\frac{\partial T(t)}{\partial t}=0 \quad (2)$$

Considering the geometric symmetry of the work roll, Eq. (2) can be further simplified to a two-dimensional problem as Eq. (3) by neglecting the heat conduction along the longitudinal direction of work roll.

$$\frac{1}{r}\frac{\partial}{\partial r}\left(K_w r\frac{\partial T(t)}{\partial r}\right)+\frac{1}{r^2}\frac{\partial}{\partial \theta}\left(K_w\frac{\partial T(t)}{\partial \theta}\right)-\rho_w C_w\frac{\partial T(t)}{\partial t}=0 \quad (3)$$

2.2 Thermal boundary conditions

Initial thermal conditions of the work roll during hot rolling can be expressed as [7,30]

$$T(r,\theta,z,t)|_{t,z=0}=T_0 \quad (4)$$

where T_0 means the initial work roll temperature before hot rolling process.

Because hot rolling is a cyclical thermal/mechanical loading problem, the thermal boundary conditions can be illustrated as shown in Fig. 1a based on a two-dimensional assumption as described in Eq. (3). Along the circumferential direction of the work roll, eight zones have been divided in a counter clockwise, namely roll bite region, wiper cooling region, nozzle spraying region, natural air cooling region, work roll and backup roll contact region, natural air cooling region, nozzle spraying region and wiper cooling region. It should be noted that practical hot rolling process in industry includes two processes, namely hot rolling and subsequent idling. In hot rolling process, there is strip-roll contact in the roll bite region, but there is no strip-roll contact in the

subsequent idling process. Therefore, the boundary conditions of hot rolling and idling are different as shown in the following section.

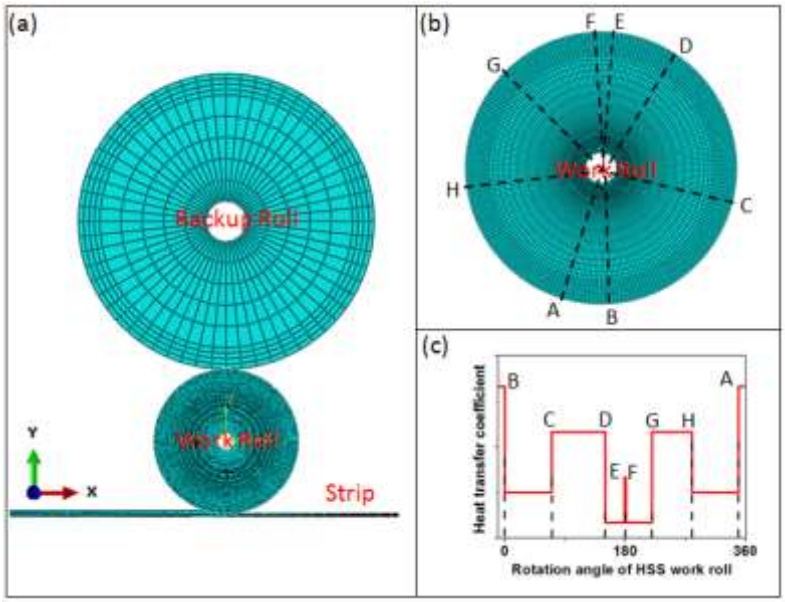

Fig. 1 Schematic of a hot rolling mill (HSM) system investigated in this study. (a) Simplified assembly of a backup roll, HSS work roll and hot strip during hot rolling, (b) detailed mesh condition of the HSS work roll and its circumferential thermal boundary conditions, and (c) illustration of corresponding heat transfer coefficients for each zone shown in (b).

2.2.1 Boundary condition in roll bite region

2.2.1.1 During hot rolling

During hot rolling, temperature rise is mainly due to conduction of heat between strip and roll. There are two heat sources in the roll bite region: deformation heating from strip being rolled, and friction heating due to sliding of the work roll on strip. Therefore, the total heat flux (q_w) into the work roll in the roll bite region can be divided into two parts: the deformation heat flux (q_d) and friction heat flux (q_f). The following boundary condition has been assumed by introducing an effective interface heat transfer coefficient (h_{con}) in roll bite region [1,31,32,47],

$$q_w = q_d + q_f = h_{con}(T_s - T(t)) \tag{5}$$

(i) The deformation heat flux (q_d) can be calculated by

$$q_d = (T_m - T(t))\frac{\delta_w}{2} C_w \rho_w v_w \tag{6}$$

where T_w means temperature at work roll surface before entering roll bite region; C_w and ρ_w means the specific heat and density of the work roll material, respectively; $v_w$means the work roll velocity; T_m means the equilibrium temperature at the work roll surface and hot strip interface, and it can be calculated as

$$T_m = \left[T_w \frac{\delta_w}{2} C_w \rho_w + (T_s + 0.5\Delta T_{sd}) \frac{\delta_s}{2} C_s \rho_s\right] / \left[\frac{\delta_w}{2} C_w \rho_w + \frac{\delta_s}{2} C_s \rho_s\right] \quad (7)$$

where $\delta_w = 2\sqrt{\alpha_w \tau_w}$ and $\delta_s = 2\sqrt{\alpha_s \tau_s}$ means penetration depth of the interface heat at the work roll and strip surface, respectively; C_s and ρ_s means the specific heat and density of the strip material, respectively; T_s means temperature at hot strip surface before entering roll bite region; ΔT_{sd} means the temperature rise of strip due to the deformation heat and can be calculated as

$$\Delta T_{sd} = \left(0.5P \frac{h_0 - h_f}{2}\right) / \left[C_s \rho_s (h_0 + h_f)/4\right] \quad (8)$$

where P is rolling pressure; h_0 and h_f are the strip thickness at the entry and exit of roll bite region, respectively.

(ii) The friction heat flux (q_f) can be calculated by

$$q_f = \left[\frac{(v - v_0)}{4} \mu P l_d / v_w\right] / \left(\frac{\delta_w}{2} C_w \rho_w + \frac{\delta_s}{2} C_s \rho_s\right) \frac{\delta_w}{2} C_w \rho_w v_w \quad (9)$$

where μ means friction coefficient between work roll and hot strip, and can be calculated in terms of a function of temperature [31]

$$\mu = -0.0714 + 4.86 \times 10^{-4} T_s \quad (10)$$

Therefore, based on Eq. (6) and Eq. (9), the total heat flux into the work roll in roll bite region during hot rolling can be calculated with the following equation

$$q_w = q_d + q_f = (T_m - T_w) \frac{\delta_w}{2} C_w \rho_w v_w + \frac{\left(\frac{(v - v_0)}{4} \mu P l_d / v_w\right)}{\left(\frac{\delta_w}{2} C_w \rho_w + \frac{\delta_s}{2} C_s \rho_s\right) \frac{\delta_w}{2} C_w \rho_w v_w} \quad (11)$$

Therefore, an effective interface heat transfer coefficient (h_{con}) in roll bite during hot rolling can be calculated by

$$h_{con} = \left[(T_m - T_w) \frac{\delta_w}{2} C_w \rho_w v_w + \frac{\left(\frac{q_f}{v_w}\right)}{\left(\frac{\delta_w}{2} C_w \rho_w + \frac{\delta_s}{2} C_s \rho_s\right) \frac{\delta_w}{2} C_w \rho_w v_w}\right] \Big/ (T_\infty - T_{w0}) \quad (12)$$

2.2.1.2 During idling

During idling, the work roll was not in contact with hot strip. The main heat loss from the work roll should be attributed to the heat convection from the work roll to the surrounded wiper coolant. The following boundary condition in this region is assumed:

$$q_{idling} = h_{idling}\big(T(t) - T_{sp}\big) \tag{13}$$

h_{idling} is the convective heat transfer coefficient of coolant in roll bite region during idling, which can be calculated by the following equation

$$h_{idling} = 0.023R_e^{0.8}P_{rcw}^{0.4}\frac{k_{cw}}{l_r} \tag{14}$$

$$R_e = v_w l_r / v_{cw} \tag{15}$$

in which k_{cw} is the thermal conductivity of coolant, l_r is the contact length in roll bite region, P_{crw} is the coolant Prandtl number, and v_{cw} is the viscosity of the coolant.

2.2.2 Boundary condition in wiper cooling regions

The surface of work roll is in contact with the coolant flowing at the wiper section. At those regions, the coolant is under atmospheric pressure compared with that under high pressure in nozzle spraying region. The following boundary condition can be used [1,30-32]

$$q_{cw} = h_{wiper}\big(T(t) - T_{sp}\big) \tag{16}$$

h_{wiper} is the convective heat transfer coefficient of coolant at the wiper region, which can be calculated by the following equation

$$h_{cw} = 0.023R_e^{0.8}P_{rcw}^{0.4}\frac{k_{cw}}{l_c} \tag{17}$$

$$R_e = v_w l_c / v_{cw} \tag{18}$$

where l_c is the coolant length along roll circumference at wiper region.

2.2.3 Boundary condition in nozzle spraying regions

The most significant heat loss from the work roll occurs in the coolant nozzle spraying region. The heat transfer coefficient in the spraying coolant region is mainly influenced by the coolant flow rate, pressure, work roll surface temperature and the geometric spray conditions in terms of spray angle with work roll surface and nozzle distance from the work roll. The following boundary condition exists in this region [1,16,31,47,48]:

$$q_{sp} = h_{spray}\big(T(t) - T_{sp}\big) \tag{19}$$

where h_{spray} is the convective heat transfer coefficient of spraying coolant at nozzle spraying region, T_{sp} is the spraying coolant temperature.

The convective heat transfer coefficient is calculated by the following equation

$$h_{spray} = 6870W^{0.19}P_{sp}^{0.27} \qquad (T(t) \le 100\ ^{\circ}\mathrm{C}) \tag{20}$$

$$h_{spray} = 2900000W^{0.08}P_{sp}^{0.05}\frac{T(t)-100}{100}\frac{B}{T(t)-T_{sp}} + 6870W^{0.19}P_{sp}^{0.27}\frac{200-T(t)}{100}\,(T(t) > 100\,℃) \quad (21)$$

where P_{sp} is the spraying coolant pressure; $W = V_{sp}/A_{sp}$ is the coolant flow per unit area created on work roll surface where V_{sp} is the coolant flow of the nozzle and A_{sp} is the coolant flow area created on work roll surface; B is taken as 1 when W is larger than 10000, otherwise $B = \left(\frac{T_{sp}}{16}\right)^{-0.17}$.

2.2.4 Boundary condition in natural air cooling regions

In the natural air cooling region, the heat loss from the work roll surface is assumed to take place by convection and radiation [30]

$$q_a = h_a(T(t) - T_\infty) + \sigma\varepsilon(T(t)^4 - T_\infty^4) \quad (22)$$

where h_a is the convective heat transfer coefficient in air and it is usually taken as a constant of 4.55~12.15 W/m^2·K; T_∞ is the surrounding temperature; σ is Stephan-Boltzmann radiation constant of black body; ε is emissivity of the work roll material.

2.2.5 Boundary condition in work/backup rolls contact region

As reported in the studies [31,32], the boundary condition at the interface between work and backup roll can be assumed as

$$q_{wb} = h_{wb}(T(t) - T_b) \quad (23)$$

in which h_{wb} is the effective heat transfer coefficient at the interface between the work roll and backup roll, T_b is the surface temperature of backup roll. The value of h_{wb} can be determined by

$$h_{wb} = \frac{0.28k_w}{\Delta\theta_{wb}R_w\sqrt{\pi\alpha_w}}\sqrt{2.256v_w\sqrt{\frac{F}{W}\frac{R_wR_b}{R_w+R_b}\left(\frac{1-\nu_w^2}{E_w}+\frac{1-\nu_b^2}{E_b}\right)}} \quad (24)$$

where $\Delta\theta_{wb}$ is the angle connection between the work and backup rolls during hot rolling.

3. Finite element analysis

3.1 Finite element model

As described in Eq. (3), a two-dimensional finite element model can be reasonably assumed to study the thermal problem of the work roll during hot rolling, by neglecting the temperature variation along the longitudinal direction [4,7,8,30-32]. In this study, a similar two-dimensional assumption has been applied in a finite element model and the schematic

illustration is shown in Fig. 1(a). Fully coupled thermal-stress analysis has been conducted using a commercial FE solver Abaqus/Standard in this study to investigate the temperature and thermal stress evolutions of a HSS work roll during hot rolling in industrial service conditions.

Table1
Practical hot rolling parameters collected from a hot strip mill finishing stands of an industrial steel company used in the models in this study.

Parameters	Stand F1	Stand F2	Stand F3	Stand F4
Rolling force	17780 kN	14940 kN	12270 kN	8510 kN
Diameter of work roll	760.8 mm	766.8 mm	790.9 mm	627.4 mm
Length of work roll	1580 mm	1580 mm	1580 mm	1580 mm
Diameter of back-up roll	1600 mm	1450 mm	1480 mm	1330 mm
Length of back-up roll	1560 mm	1560 mm	1560 mm	1560 mm
Velocity of work roll	1.36 m/s	2.15 m/s	3.34 m/s	4.82 m/s
Strip temperature before hot rolling	973 °C	955 °C	942 °C	927 °C
Strip temperature after hot rolling	955 °C	942 °C	927 °C	913 °C
Strip thickness before hot rolling	40 mm	20.25 mm	12.44 mm	8.15 mm
Strip thickness after hot rolling	20.25 mm	12.44 mm	8.15 mm	5.82 mm
Strip width before hot rolling	1136 mm	1141 mm	1145 mm	1147 mm
Hot rolling reduction per pass	49.38%	38.57%	34.49%	28.59%
Nozzle water spraying pressure	1.25 MPa	1.25 MPa	1.20 MPa	1.15 MPa

Formatted: Left, Space Before: 0.5 line

Detailed thermal boundary conditions along the circumferential direction of the work roll are shown in Fig. 1(b), where 8 regions have been divided as marked. Region AB indicates the roll bite region, regions BC and HA indicate the wiper cooling regions, regions CD and GH indicate the nozzle spraying regions, regions DE and FG indicate the natural air cooling regions, and region EF indicates the contact between the work roll and back-up roll. During finite element analysis, the above mentioned thermal boundary conditions were defined in a user subroutine FILM [49], which can be used to define a node/element/surface-based non-

uniform film coefficient and will be called during procedures that allow heat transfer analysis at each node or surface integration point.

This study was focused on the four front finishing stands (F1, F2, F3 and F4) in a hot strip mill, where HSS work rolls are used. The roll was assumed as deformable body, and its physical and mechanical properties are shown in Table 1, 2 and 3, respectively. In order to avoid the convergence problem during simulation, a small hole with diameter of 20 mm (R_0=20 mm) in the work roll center was removed when building the finite element model. As can be seen in Fig. 1(b), very fine mesh was used in the outer layer of the work roll and coarse mesh was used inside to improve the calculation accuracy of work roll surface temperature. The element type for the work roll was CPE4T, namely four-node plane strain thermally coupled quadrilateral, bilinear displacement, and temperature [49].

3.2 Analysis procedures

Detailed finite element analysis procedures in this study are given as following:

Step 1: Collecting industrial parameters, including physical and mechanical properties of strip, work and back-up rolls, and rolls geometry dimensions, rolling pressure, roll speed and so on, from practical steel hot rolling industry company as listed in Table 1 and Table 2, respectively.

Step 2: Identifying the heat transfer coefficients at different boundary conditions as described in Section 2.2 based on the above collected industrial parameters and experimental parameters in [5].

Step 3: Building finite element models to simulate the hot rolling experiment reported by Steven et al. [5] and validating the models by comparing the simulation results and their experimental measurements.

Step 4: Conducting finite element analysis on the thermal behaviour (temperature and thermal stress evolutions) of a HSS work roll based on practical steel hot rolling conditions.

Step 5: Investigating the influencing factors, such as finishing stand number F1-F4, heat transfer coefficients in different thermal boundary regions and initial work roll body temperature.

Step 6: Calculating the working temperature at the HSS work roll surface during hot rolling for further investigation on oxidation behaviour of the HSS work roll material.

Table 2

Physical and mechanical properties of the work roll and back-up roll used in the FE models in this study [2,5,21,30,50,51].

Roll material type	HSS	Cr5	S.G. cast steel
Thermal conductivity	27.3 W/m·K	43.5 W/m·K	32.4 W/m·K
Specific heat capacity	462 J/kg·K	448 J/kg·K	743 J/kg·K
Density	7620 Kg/m^3	7837 Kg/m^3	7200 Kg/m^3
Elastic modulus	220 GPa	205 GPa	176.7 GPa
Thermal expansion coefficient	1.4×10^{-5} K^{-1}	1.7×10^{-5} K^{-1}	1.25×10^{-5} K^{-1}
Poisson's ratio	0.3	0.3	0.275
Tensile strength	800 MPa	1916 MPa	263.5 MPa
Compressive strength	3200 MPa	1620 MPa	1317.4 MPa

4. Experimental details

4.1 On-site measurement of work roll temperature [5]

Due to the complicated operations and extremely high cost of on-site work roll temperature measurement, the report by Stevens et al. [5] has been the unique available industrial experiment. Therefore, simulating their experiment is very important and should be conducted first to validate the models. Details of their experimental set-up were simply recalled in this section.

In Ref. [5], a full-scale S.G. cast iron work roll was modified firstly and fitted with five thermocouples at different depths from the work roll surface to measure the corresponding temperature distributions. Two identical plugs were installed in order to avoid failure of any of the thermocouples. Then, the modified roll was fitted on several occasions into the No. 2 roughing stand of the No. 1 medium width strip mill of the BSC Tubes Division at Corby. Finally, practical hot rolling of slabs was conducted and a typical set of temperature distributions were recorded. In their hot rolling experiment, the work roll had an angular speed of 12.8 rpm and initial temperature of 20 ^{o}C. Temperatures of the slabs were 1230 ^{o}C on the entry side, and the rolling reduction was 22.75% per pass with rolling pressure of 108.5 MPa. The industrial experiment was conducted up to 5 hours for testing temperature variations both at the surface and within main body of the work roll.

4.2 High temperature oxidation test

In addition to systematically understanding temperature and thermal stress evolutions in a HSS work roll during hot rolling in industry, another important goal of this study is to understand the oxidation behaviour of the HSS work rolls during hot rolling in actual service condition. Due to extremely difficult and complicated operations, it is impossible to examine the oxidation of work rolls during industrial hot rolling operations. Therefore, oxidation experiment of the HSS work roll materials has been conducted in laboratory. Table 1 shows the chemical composition of the material investigated in this study. Samples with dimensions of 12 × 12 ×6 mm^3 were cut from a HSS work roll in actual service condition. Sample surface was polished with a 1 um diamond suspension and the roughness was about 17 nm. All samples were ultrasonically cleaned with acetone and kept in vacuum before the oxidation experiment. Four different oxidation temperatures from 550 to 700°C have been selected in this study. The overall oxidation time was set to 10 and 30 minutes, which are comparable to the practical strip-roll contact time during industrial hot strip rolling process.

Table 3
Chemical compositions of the investigated HSS work roll, Cr5 backup roll and strip materials during hot rolling in this study, wt.%.

Material	C	Mn	Si	Ni	Cr	Cu	Mo	Al	V	W	Fe
HSS	1.78	0.551	0.69	0.52	5.0	0.080	3.7	0.005	5.2	0.2	Bal.
5%Cr	0.7	0.5	0.6	0.4	5.2	-	0.5	-	0.2	-	Bal.
Strip	0.032	0.25	0.009	0.01	0.01	0.02	-	-	0.001	-	Bal.

4.3 Characterization of oxide scales

Surface morphology of all the oxidized HSS samples was characterized with a help of a JEOL JSM-6490 scanning electron microscopy (SEM). In addition, a FEI XT Nova Nanolab 200 work station combining a dual beam of focused ion beam (FIB) and a field emission scanning electron microscope was used to cut samples along the oxide scale thickness direction. They were further observed by a JEOL JEM-ARM200F probe corrected scanning transmission electron microscope (STEM) with an accelerating voltage of 200 kV. Microstructure of the oxide scale formed at a HSS work roll surface during practical steel hot rolling in industry was also examined for a comparison.

5. Results and discussion

5.1 On-site temperature measurement and model validation

In this section, simulated temperature evolution in a S.G. iron steel work roll based on the experimental condition in industry [5] has been shown, and a comparison with their on-site measurement has been made in order to validate the developed model.

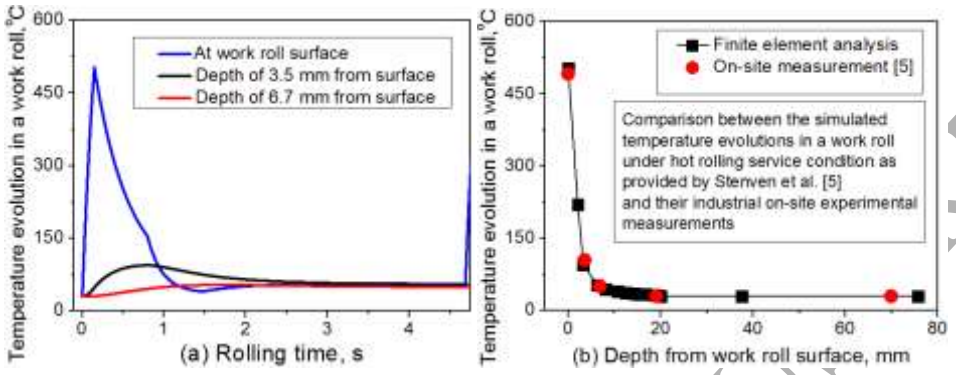

Fig. 2 (a) Simulated temperature evolution histories at three different depths in a S.G. iron steel work roll under industrial hot rolling service condition as provided by Steven et al. [5], and (b) comparison between the simulated results in this study and their on-site experimental measurements.

Fig. 2a shows the simulated temperature evolution history of three selected depths from work roll surface during one revolution of hot rolling. As can be seen, the temperature at the roll surface increases rapidly from 20 °C to 510.8 °C during contact with hot slab having initial temperature of 1230 °C, and then decreases gradually due to the subsequent water cooling and natural air cooling. The minimum temperature is about 50 °C at the end of revolution. By contrast, the temperatures at depth of 3.5 mm and 6.7 mm from the roll surface are much lower than at surface. The temperature rise rate in a work roll decreases significantly with depth, and the maximum temperatures obtained during one revolution are 105.2 °C at depth of 3.5 mm and 63.5 °C at depth of 6.7 mm, respectively. In the report [5], the measured temperature at surface was about 500 °C during the first revolution, which is slightly lower than the present simulation result. This can be attributed to the experimental errors by operations and sensitivity of the thermocouples.

In Fig.2b, a direct comparison between the finite element simulation and practical on-site measurement has been made, in terms of the temperature distribution in the work roll along its radial direction. Very good agreement between the simulation and experiment indicates that the developed finite element model is able to reasonably capture the temperature evolution in a S.G. cast iron work roll during hot rolling. This method will be further used to study the thermal behaviour of a HSS work roll during hot rolling.

5.2 Simulated temperature evolution in a HSS work roll

As validated in the section 5.1, finite element model has very good capacity to study the temperature evolution in a work roll during hot rolling. Simulations based on the industrial condition as listed in Table 1 have been conducted.

Table 4
Heat transfer coefficients used in the FE models to understand the influence of thermal boundary conditions on the temperature and thermal stress evolution in a HSS work roll during hot rolling in actual service condition.

Case no.	h_{con} (kW/m^2·K)	h_{wiper} (kW/m^2·K)	h_{spray} (kW/m^2·K)	h_a (W/m^2·K)
1	10	1	35	10
2	25	1	35	10
3	40	1	35	10
4	50	1	35	10
5	75	1	35	10
6	100	1	35	10
7	150	1	35	10
8	50	0.1	35	10
9	50	5	35	10
10	50	10	35	10
11	50	15	35	10
12	50	35	35	10
13	50	1	5	10
14	50	1	15	10
15	50	1	25	10
16	50	1	45	10
17	50	1	55	10

Formatted: Left, Space Before: 0.5 line

5.2.1 Temperature evolution at different finishing stands

HSS work rolls were only applied in the first four finishing stands (F1-F4) in the studied hot strip mill as suggested by our industrial collaborators. Therefore finite element simulations only about these four stands have been conducted.

Based on the industrial hot rolling service conditions, temperature evolution at work roll surface has been analysed using the finite element method as introduced in Section 2. Fig. 3a shows the simulated temperature evolution history at the HSS work roll surface during the first hot rolling revolution at stand F1 to F4. As can be seen, time required for one rolling revolution decreases gradually with the stand number, which is about 1.75 seconds at stand F1 but only about 0.4 seconds at stand F4. This is attributed to the different work roll velocities, work roll dimensions and rolling reductions as shown in Table 2. For all four stands, temperature at the work roll surface increases rapidly when contact with the hot strip is established in the roll bite region. Fig. 3b is the highlighted part in Fig. 3a, which shows the maximum temperatures reached at HSS work roll surface during one rolling revolution. They are about 581.3 °C at stand F1, 525.5 °C at stand F2, 442.4 °C at stand F3, and 340.1 °C at stand F4, respectively. Those results indicated that the maximum temperature at the work roll surface is highly dependent on the number of stands, which means a large influence on the thermal stress distribution, oxidation behavior and service life of a HSS work roll [2]. The larger maximum surface temperatures at earlier stands are due to the longer roll-strip contact time, higher strip temperature and slower strip speed.

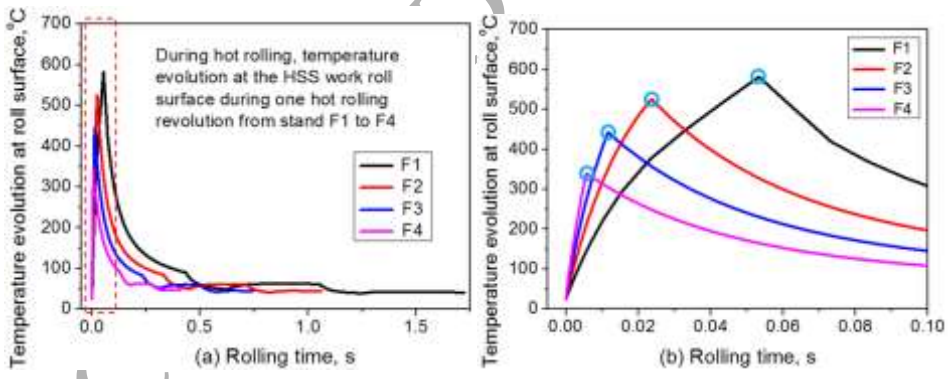

Fig. 3 Variation of temperature at the HSS work roll surface in the finishing stands F1-F4 of a hot strip mill. (a) Temperature evolution histories at the HSS work roll surface during the first hot rolling revolution, and (b) highlighted the temperature evolutions at work roll surface during contact with strip as marked in (a) during hot rolling.

5.2.2 Influence of hot rolling parameters on temperature evolution

Based on the comparison of results shown in Fig. 3, stand F1 which has the largest peak temperature has been selected in this study for further investigating the influence of thermal boundaries on the temperature evolution in a HSS work roll during hot rolling.

As introduced in section 2, thermal boundaries of hot rolling are very complicated and can be influenced by many factors. In this study, the main influences of h_{con} varying from 10 to 150 kW/m^2·K in the roll bite region, h_{wiper} varying from 0.1 to 35 kW/m^2·K in the wiper cooling regions, and h_{spray} varying from 5 to 55 kW/m^2·K in the nozzle spraying cooling regions as shown in Table 4 are carefully studied.

Fig. 4a shows the relationship between temperature evolution history at the HSS work roll surface during one revolution and the value of coefficienth_{con}. As can be seen from the figure, there is a significant influence, particularly on the maximum temperature obtained at roll surface at the exit of roll bite region marked as position B. From the summary in Fig. 4b, the maximum temperature rises linearly with h_{con}, and the rise rate decreases when h_{con} is larger than 60 kW/m^2·K. The maximum temperature is about 200 °C at h_{con} of 10 kW/m^2·K, and about 850 °C at h_{con} of 150 kW/m^2·K. In addition, a larger h_{con} also leads to a higher temperature in region BC, which indicates that the HSS work roll undergoes a longer oxidation at a higher temperature.

Fig. 4c shows the influence of h_{wiper} in the wiper cooling regions BC and HA. The results suggest that the maximum temperature is not influenced because of the constant h_{con} and roll-strip contact time in region AB, but there is a large temperature difference in region BC. At position C, the temperature is about 50 °C at h_{wiper} of 0.1 kW/m^2·K, and 150 °C at h_{wiper} of 35 kW/m^2·K, respectively. By comparison, Fig. 4d shows that h_{spray} has a much smaller influence on the temperature at the HSS work roll surface. The smaller h_{spray} leads to a continuous temperature decrease at roll surface when the roll leaves nozzle spraying cooling region at position D, but a temperature rise has been observed at position D at a larger h_{spray}. These results suggest a complicated thermal stress state and will be discussed in section 5.3.

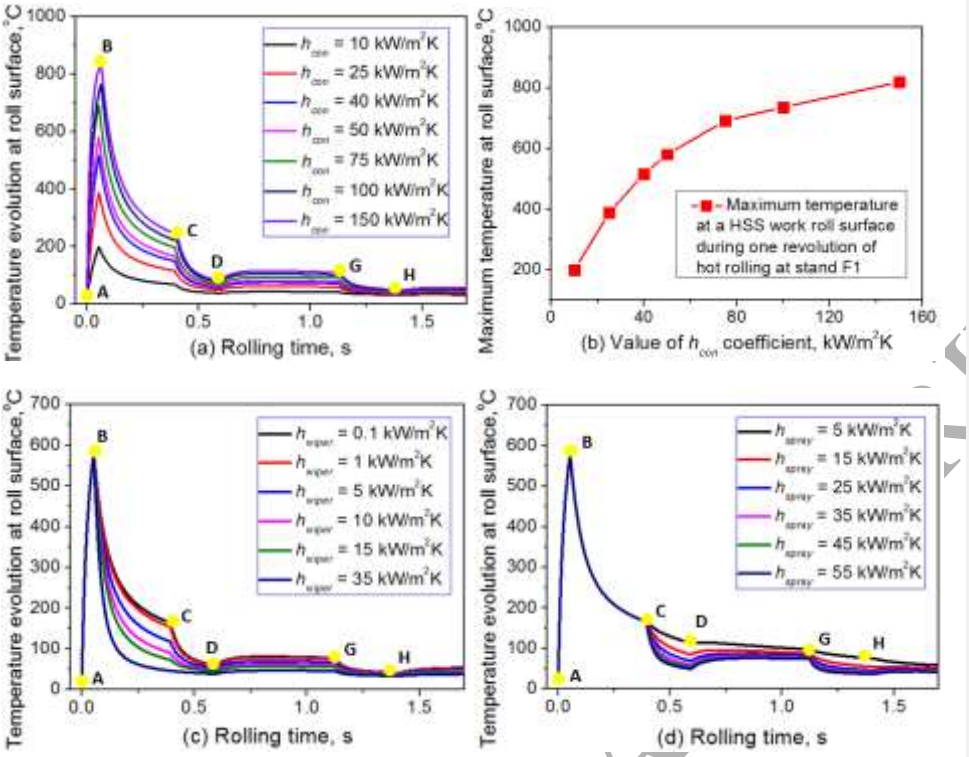

Fig. 4 (a) Influence of coefficient h_{con}in roll bite region, (b) the maximum temperature obtained at roll surface in (a), (c) influence of coefficient h_{wiper} in wiper cooling regions, and (d) influence of coefficient h_{spray} in the nozzle cooling regions on the temperature evolution history at a HSS work roll surface during one revolution of hot rolling.

5.2.3 Influence of initial work roll body temperature

In fact, the available reports on the temperature field of a work roll during hot rolling are not consistent with each other. One of the main reasons is the different initial temperatures of roll body, and very limited studies have considered its influence. For example, the initial roll body temperature was assumed as 30 °C by Li et al. [18,19], 100 °C by Sun et al. [21], 150 °C by Benasciutti et al. [29], and 200 °C by Chang [22], respectively. Up to now, only Na et al. [30] have studied the influence of initial roll body temperature. However, they have only focused on the 7th stand of a hot strip rolling mill, where the maximum temperature at roll surface was very low (only about 300 °C) and it is not high enough for investigation of oxidation behavior of a work roll. Therefore, this study provides the first consideration on the influence of initial roll body temperature at stand F1 of a hot strip rolling mill, which is very important to understand the thermal stress evolution and oxidation in a HSS work roll.

In this study, temperature evolutions during both hot rolling and subsequent idling have been studied in detail by assuming initial roll body temperature as 25, 100 and 200 °C,

respectively. Fig. 5 shows the temperature distribution in the cross-section of a HSS work roll at the end of hot rolling one strip and subsequent idling. By comparing the results in Fig. 5a, c and e, it can be observed that temperature decreases gradually from the roll surface along its radial direction for all three initial roll body temperatures, which can also be found in Fig. 6a by plotting temperature as a function of depth from roll surface at the end of hot rolling. In addition, large temperature gradient only exists close to the surface within depth of 10 mm. A careful examination indicates that the initial body temperature has a slight influence on the maximum temperature, which increases gradually and reaches to about 650 °C at roll surface when the initial temperature is 200 °C.

Opposite to the small influence during hot rolling, a large difference in temperature distribution in the work roll has been observed during idling. Fig. 5b shows the cross-section of temperature contour at the end of idling for initial temperature of 25 °C. The figure reveals that the temperature at roll surface is lower than its subsurface layer, which should be attributed to the water and natural air cooling. From Fig. 6b, the temperature increases gradually from 35 °C at the roll surface when the depth is smaller than about 20 mm, but decreases again with increasing depth and reaches to stable at depth of 100 mm. The result for initial roll body temperature of 100 °C is quite similar to that of 25 °C as shown in Fig. 5d and Fig. 6b, where the minimum temperature is about 40 °C at the roll surface, while the maximum temperature is about 135 °C at depth of 25 mm. It should be noted that Fig. 6f shows an obvious different trend for initial roll body temperature of 200 °C by comparing with Fig. 5b and d. The temperature increases from about 40 °C at surface and reaches to about 200 °C at depth of 50 mm, and no obvious temperature drop in the HSS work roll has been observed with further increasing depth.

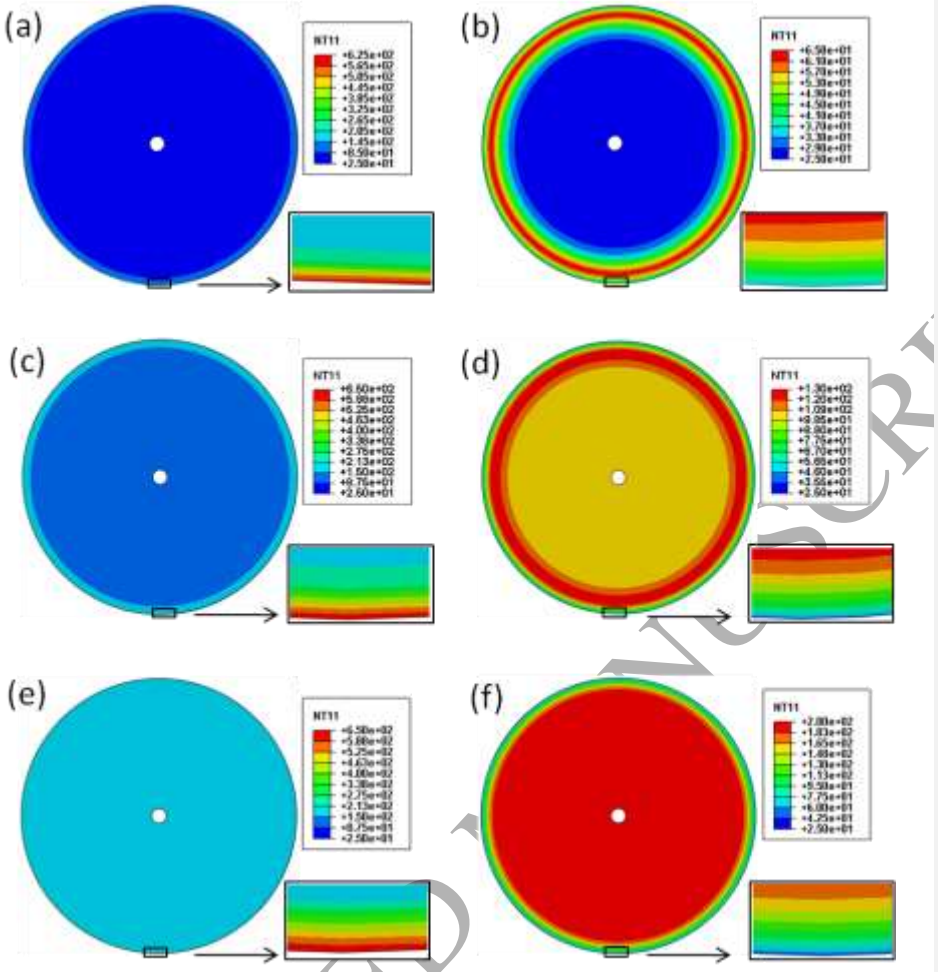

Fig. 5 Influence of initial roll body temperature on the temperature evolution in a work roll during hot rolling and subsequent idling. Temperature contours in the cross-section of a HSS work roll at the end of hot rolling one strip, with initial roll body temperature of (a) 25 °C, (c) 100 °C, and (e) 200 °C; at the end of idling after hot rolling one strip with initial roll body temperature of (b) 25 °C, (d) 100 °C, and (f) 200 °C.

The results indicate that the Influence of initial roll body temperature on the temperature evolution in a HSS work roll during both hot rolling and subsequent idling in this study is consistent with the earlier report by Na et al. [30]. However, the maximum temperature is much higher in this study than their results, because this study focused on stand F1 while the latter focused on stand F7. In our previous work [4], it has been shown that the maximum temperature of 628 °C was obtained at roll surface during hot rolling one strip when the roll body had an initial temperature of 25 °C. By contrast, the maximum temperature at roll surface during hot rolling one strip was about 647.1 and 651.9 °C when the initial roll body temperature increased to 100 and 200 °C, respectively, as shown in Fig.

6a. It is therefore the working temperature range at a HSS work roll surface at stand F1 from 581.3 to 651.9 °C during hot rolling can be concluded from the above modeling analysis.

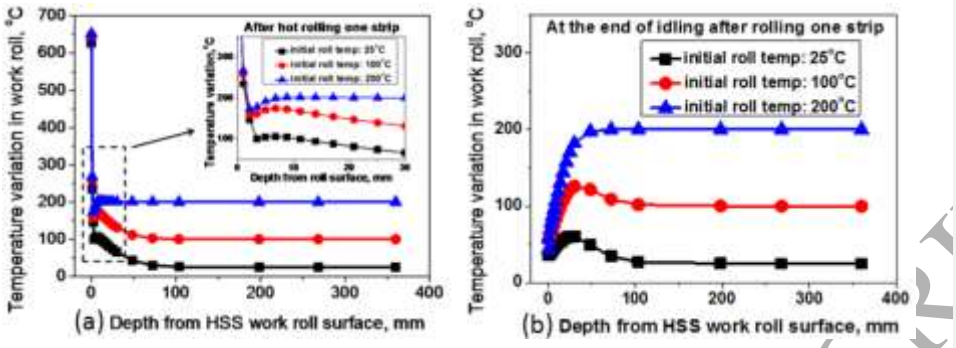

Fig. 6 Influence of initial roll body temperature on the temperature distribution along the HSS work roll radial direction at the end of (a) hot rolling one strip, and (b) subsequent idling.

5.3 Analysis of thermal stress evolution

5.3.1 Thermal stress evolution during hot rolling

Fig. 7a shows the thermal stress evolution history of three selected depths, namely at roll surface, depth of 2 mm and 5 mm, in a HSS work roll during one revolution of hot rolling at stand F1 in actual service conditions. As can be seen, very large compressive circumferential thermal stress of 950 MPa has been introduced at roll surface due to contact with hot strip in the roll bite region AB. Then, the compressive thermal stress decreases continuously due to the wiper cooling in region BC and nozzle spraying cooling in region CD. The stress is about -205 MPa at position C, -150 MPa at position D, -160 MPa at position G, and -53 MPa at the end of revolution. By contrast, the thermal stress evolutions at the other two depths are completely different from at surface. At depth of 2 mm, compressive circumferential thermal stress also develops because of the circumferential expansion is constrained by the surrounding material with lower temperature. However, the maximum thermal stress is not reached at the exit of roll bite region AB but in the subsequent wiper cooling region BC, because of the maximum temperature reached there. The magnitude of compressive stress is about 208.7 MPa, and then decreases gradually with further cooling and reached to 66.2 MPa at the end of revolution. By contrast, the compressive stress at depth of 5 mm is much lower than at surface and depth of 2 mm, and continuous stress rise can be observed in Fig. 7a. Similar phenomena have also been reported by Benasciutti et al. [29] and Na et al. [30], respectively.

The simulation results for the other three stands (F2-F4) revealed very similar thermal stress evolution trend to stand F1, suggesting a large thermal stress gradient in a very thin layer close to the roll surface. In Fig. 7b, a direct comparison of the thermal stress evolution in a HSS work roll at all four stands has been made in terms of magnitudes of the maximum compressive circumferential thermal stress obtained at roll surface during on revolution. The figure indicates that the thermal stress decreases gradually from stand F1 to F4, which is consistent with the roll surface temperature evolutions as shown in Fig. 3. As can be seen, the maximum compressive stress is about 900 MPa at stand F2, 750 MPa at stand F3, and 500 MPa at stand F4, respectively.

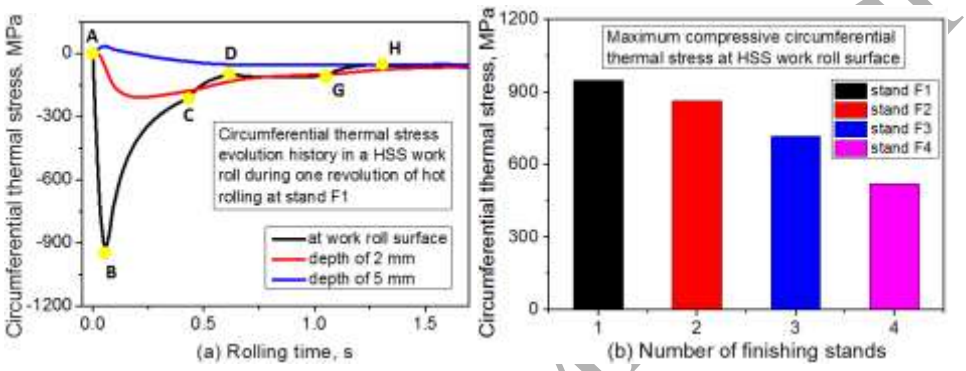

Fig. 7(a) Circumferential thermal stress evolution history at three selected depths from the HSS work roll surface during one revolution of hot rolling, and (b) comparison of the maximum compressive circumferential thermal stress obtained at the HSS work roll surface at stands F1-F4.

Fig. 8 shows the influence of thermal transfer coefficients on the thermal stress evolution in a HSS work roll. In Fig. 8a, a significant influence of h_{con} varying from 10 to 150 kW/m^2·K has been observed by examining the thermal stress evolution history at the roll surface. Compressive thermal stress was introduced for all cases due to the constrained circumferential expansion. As compared in Fig. 8d, magnitude of the peak stress increased gradually from about 357.9 MPa at h_{con} of 10 kW/m^2·K to 1641.3 MPa at h_{con} of 150 kW/m^2·K. In addition, thermal stress at surface almost does not change after position C when h_{con} is smaller than 25 kW/m^2·K, but slight stress rise in region DG can be observed when h_{con} is larger than 25 kW/m^2·K. Fig. 8b shows that a larger h_{wiper} leads to a quicker stress drop in region BC. The stress at position C was -392.4 MPa when h_{wiper} is 0.1 kW/m^2·K, but only -88.6 MPa when h_{wiper} is 35 kW/m^2·K. Similarly, stress decreases fast with increasing h_{spray} in region CD as shown in Fig. 8c. It is interesting to see that, stress does not increase but decrease continuously when h_{spray} is smaller than 15 kW/m^2·K in

region DG. This suggests that the heat conduction from the subsurface layers is lower than heat loss at surface due to cooling. The detailed stresses at the marked positions in Fig. 8 have been listed in Table 5.

Table 5
Circumferential thermal stress (σ_X) at the marked positions in Fig. 8, where X = B, C, D, G, H indicates the number of positions.

Case No.	σ_B (MPa)	σ_C (MPa)	σ_D (MPa)	σ_G (MPa)	σ_H (MPa)
1	-357.9	-112.1	-50.3	-46.2	-26.6
2	-745.2	-234.8	-97.1	-92.4	-43.3
3	-855.5	-322.6	-130.7	-125.6	-55.8
4	-978.9	-367.7	-139.8	-135.4	-59.7
5	-1314.1	-449.3	-179.8	-173.9	-74.2
6	-1466.1	-566.6	-212.6	-216.9	-84.8
7	-1641.3	-635.6	-212.6	-243.8	-94.7
8	-978.9	-392.4	-238.4	-141.2	-61.8
9	-978.9	-281.6	-115.9	-114.4	-52.1
10	-978.9	-211.7	-95.5	-95.9	-45.4
11	-978.9	-166.7	-81.5	-83.2	-40.6
12	-978.9	-88.6	-54.7	-57.6	-31.1
13	-978.9	-367.7	-272.1	-204.6	-151.3
14	-978.9	-367.7	-207.8	-173.7	-99.2
15	-978.9	-367.7	-170.5	-154.7	-75.1
16	-978.9	-367.7	-131.8	-129.5	-54.1
17	-978.9	-367.7	-120.9	-123.5	-48.9

Formatted: Left, Space Before: 0.5 line

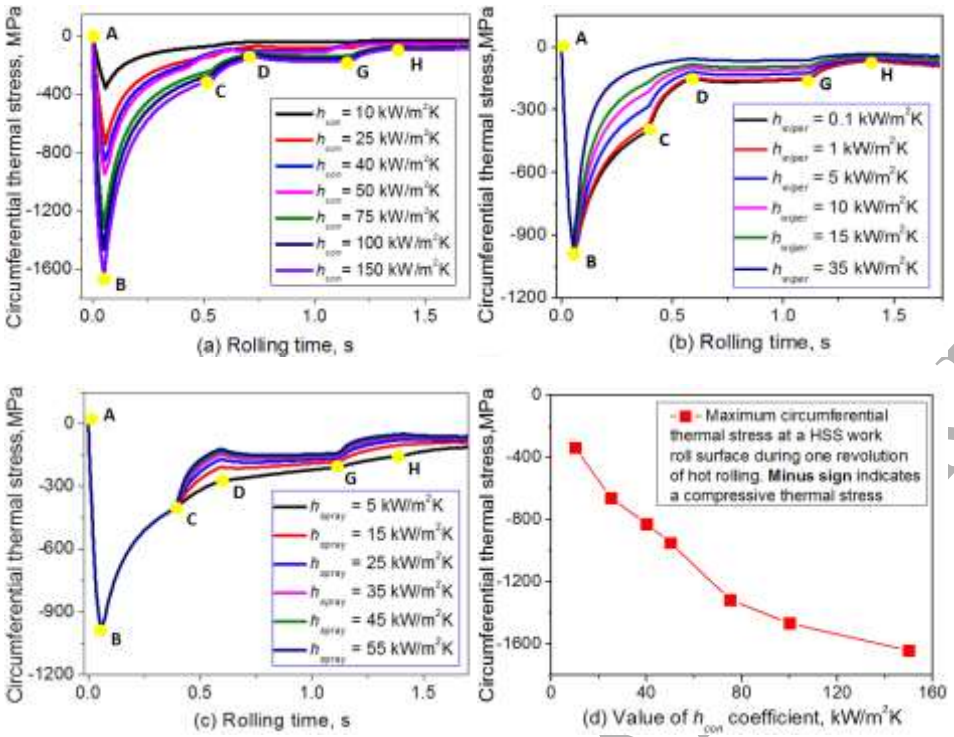

Fig. 8 Thermal stress evolution history at a HSS work roll surface at stand F1 during one revolution: (a) Influence of h_{con} in the roll bite region, (b) influence of h_{wiper} in the wiper cooling regions, (c) influence of h_{spray} in the nozzle spraying cooling regions, and (d) comparing influence of h_{con} on the maximum thermal stress reached at the HSS work roll surface. (Sign of "-" means compressive thermal stress.)

5.3.2 Thermal stress evolution during idling

In Fig. 9, the thermal stress evolution history at a HSS work roll surface during hot rolling one strip and subsequent idling has been shown, and the influence of initial roll body temperature has also been compared. Fig. 9a shows the cyclical character of stress evolution during hot rolling when initial roll body temperature is 25 °C. The roll surface undergoes compression along the circumferential direction during the whole process (namely hot rolling and idling). During hot rolling, magnitudes of the maximum and minimum stresses increase gradually from the first revolution to the eighth revolution, and then become relatively stable as reported in [4]. However, thermal stress during idling is completely different from hot rolling, where the stress decreases quickly and reaches to about 0.5 MPa at the end of idling. This result is consistent with the previous reports [19,29,30] when the initial work roll body temperature is low. With increasing the initial roll body temperature to 100 °C as shown in Fig. 9b, the HSS work roll undergoes cyclical compression and tension at surface during rolling and a relatively stable condition has been reached after six revolutions.

It has been found that the rise of initial roll body temperature leads to a decrease of the maximum compressive stress during rolling, and the decrement is about 100 MPa from the previous 950 MPa. In addition, a tensile stress of about 50 MPa has been reached at the end of each revolution during steady-state hot rolling stage. The figure also shows that the thermal stress is compressive during the early stage of idling but tensile during the rest (after about 10 seconds). The maximum tensile stress of about 150 MPa has been observed at the end of idling. With further increasing the initial roll body temperature to 200 °C as shown in Fig. 9c, a large drop of compressive stress can be observed. It is different from the previous two cases, the maximum compression stress decreases gradually from the first revolution due to the higher temperature at subsurface layers. Relative stable rolling state has been reached only after two revolutions. Similar to the result in Fig. 9b, the roll surface undergoes cyclical compression and tension during rolling, and the maximum compression stress and tensile stress are about 750 MPa and 310 MPa, respectively. The work roll surface is subjected to tension during the whole stage of idling when the initial roll body temperature is 200°C.

The maximum and minimum circumferential thermal stresses developed at the HSS work roll surface during both hot rolling and subsequent idling have been summarized in Fig. 10. As can be seen, the difference between the maximum and minimum stresses is very small during hot rolling for all three initial roll body temperatures. However, it is large during idling. The stress changes from completely compressive at initial roll body temperature of 25 °C to completely tensile at initial roll body temperature of 200 °C. Tensile stress in a work roll has also been predicted in the early reports [21,22,29]. It should be noted that the two temperatures of 25 and 200 °C are the lower bound and upper bound of the work roll body temperature during hot rolling process under industrial service conditions. Initial 25 °C only exists during the early stage of hot rolling as shown in [4], while 200 °C is very difficult to reach because the period of rolls exchange is shorten for increasing the rolls life. It is therefore the second case of initial 100 °C is more close to the practical steady-state hot rolling and the work rolls are subjective to both compression and tension in majority of the practical conditions.

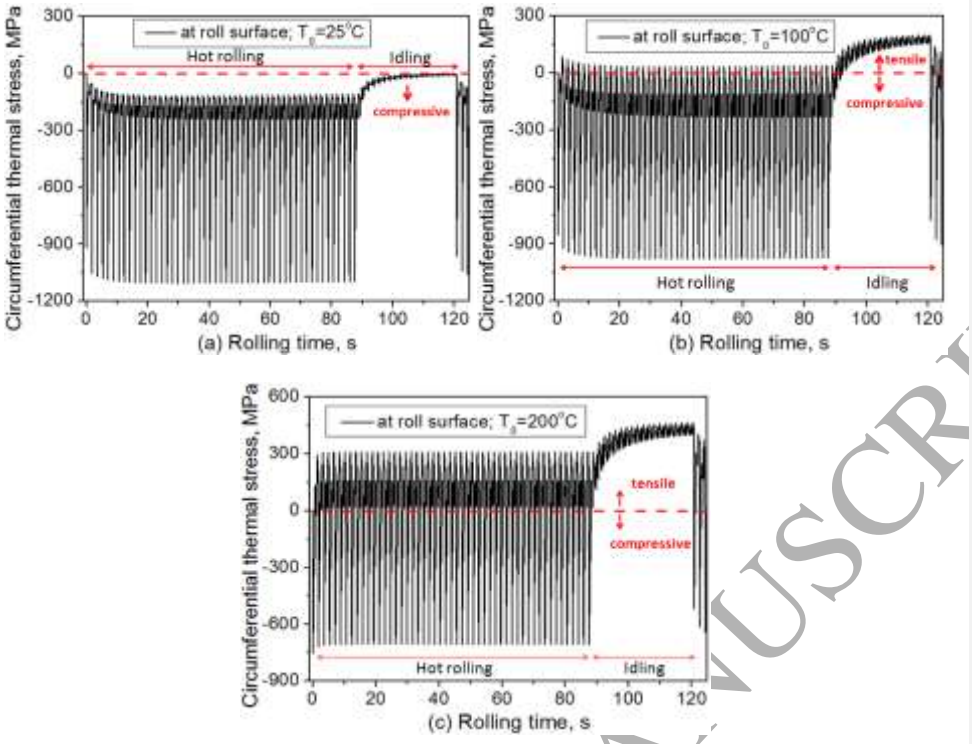

Fig. 9 Thermal stress evolution history at a HSS work roll surface during hot rolling and subsequent idling with different initial work roll body temperature of: (a) 25 °C, (b) 100 °C, and (c) 200 °C.

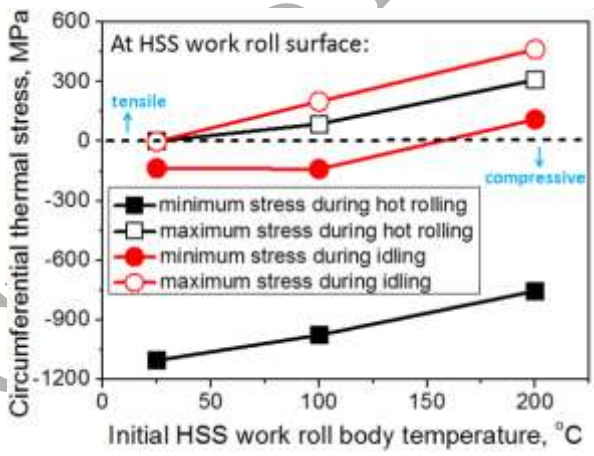

Fig. 10 Comparison of the maximum and minimum circumferential thermal stresses obtained at the HSS work roll surface during hot rolling and subsequent idling with different initial roll body temperatures.

5.4 Surface morphology of oxide scales

The typical microstructure of the HSS work roll material before high temperature oxidation test has been shown in Fig. 11a [4]. With a help of XRD and EDX analysis, vanadium rich carbides (MC), molybdenum rich carbides (M_2C), and chromium rich carbides (M_7C_3) dispersed in the matrix have been identified. From the figure, the calculated total volume fraction of all three carbides is approximately 11.4%. As revealed in the earlier reports [33-35], those carbides in a HSS material contribute on its mechanical strength and wear resistance due to their high hardness relative to the matrix.

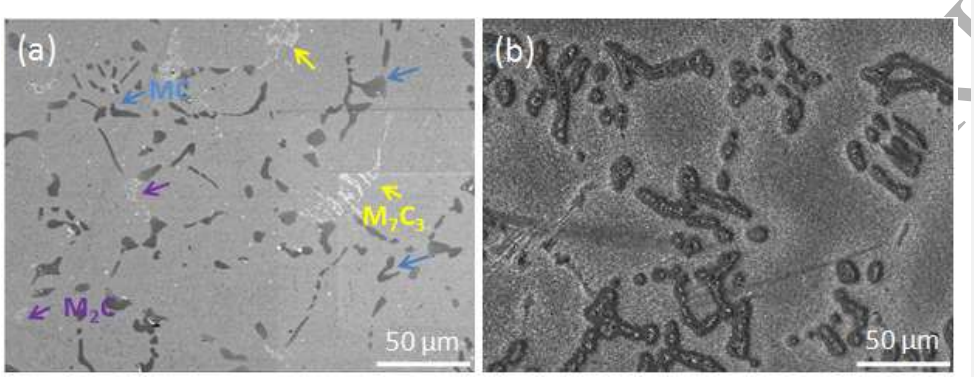

Fig. 11 Surface morphology of HSS samples observed by SEM: (a) before high temperature oxidation test [4], and (b) after oxidation at 550 °C for 10 minutes in a humid atmosphere.

According to the finite element analysis in section 5.2, it has been found that the working maximum temperature range is from 581.3 to 651.9°C at a HSS work roll surface during hot rolling at stand F1. Therefore, oxidation tests at 600°C and 650°C have been conducted in laboratory. In order to make a comparison, additional HSS samples were also oxidized at 550°C and 700°C. Fig. 11b shows the HSS sample surface morphology after oxidation at 550 °C for 10 minutes in a humid atmosphere. As can be seen, it is very difficult to detect the oxide growth on the steel matrix and only the carbides are slightly oxidized maintaining their original shapes. This observation is consistent with the study by Kim et al. [37], and it is attributed to the high free energy at the carbide/matrix interface and lower thermal stability of the carbides. In contrast, the formation and growth of oxide scales on the HSS sample surface can be clearly observed at higher temperatures as shown in Fig. 12. The morphology of HSS sample surface after oxidation at 600°C in a dry atmosphere is shown in Fig. 12a, where a compact thin oxide scale covers the HSS matrix and the carbides are oxidized and protrude above the matrix surface. Similar results for oxidation at 650°C and 700°C can be observed in Fig. 12b and c, respectively. It is evident that the height difference between the oxidized matrix and carbides increases gradually with temperature. It should be noted that

different type of carbides also have different oxidation rate as reported by Zhou and co-authors [43,44]. Their results indicated that vanadium rich MC carbides are oxidized more heavily than the chromium rich M_7C_3 carbides. According to the study by Molinari and Pellizzari [39], the Mo rich M_2C carbides have an intermediate oxidation rate.

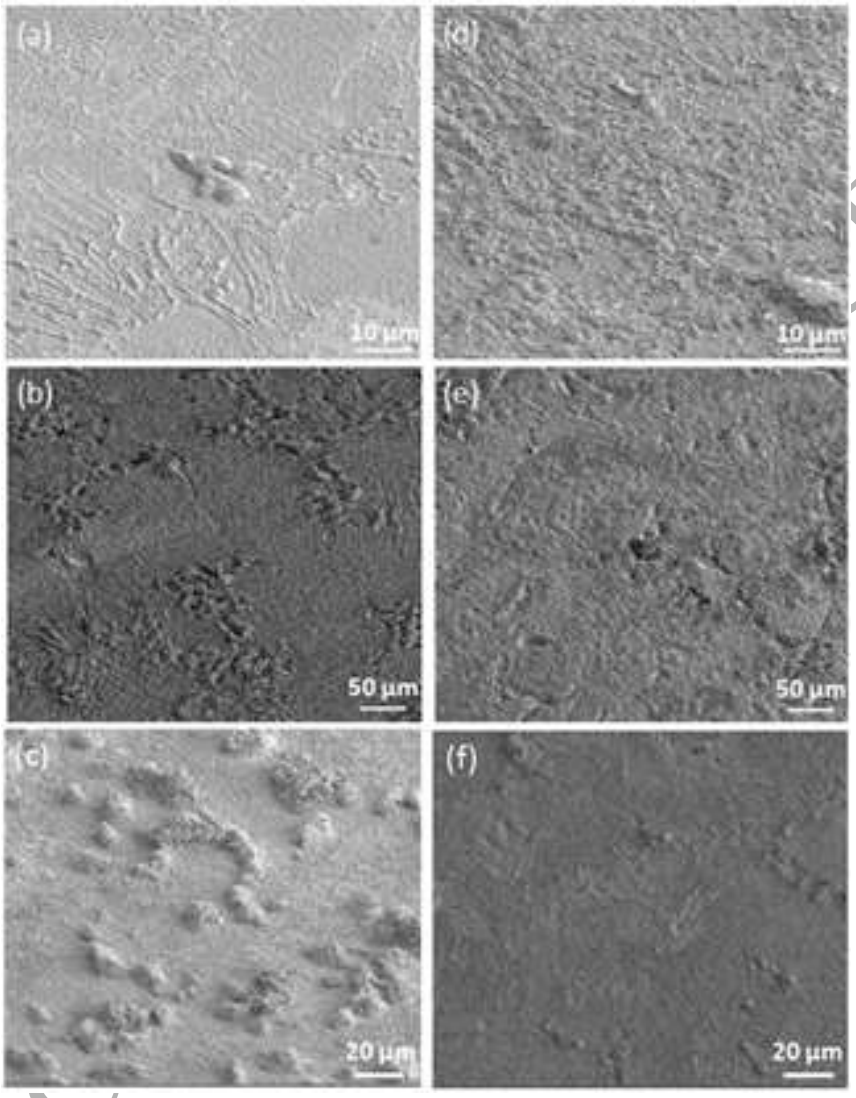

Fig. 12 Surface morphology of HSS samples oxidised for 10 minutes at temperature of (a) 600 °C, (b) 650 °C and (c) 700 °C in a dry atmosphere; and at temperature of (d) 600 °C, (e) 650 °C and (f) 700 °C in a humid atmosphere.

In addition, morphologies of the oxidized HSS sample surface at temperatures from 600 to 700°C under humid atmosphere have also been examined as shown in Fig. 12d-f. It is obvious that the humid atmosphere leads to more heavily oxidation than the dry

atmosphere at the same temperature. The figure also shows that the oxide scales under dry atmosphere are dense, but the layer developed under humid atmosphere is porous. Besides, the sample surface becomes more evenly because the water vapour improves oxidation rate of both matrix and carbides under humid atmosphere. It was proposed that the increased oxidation was due to a dissociation reaction in the pores of the oxide which contained H_2O and H_2 [52]. The presence of water vapour also prevents the development of a protective chromium oxide layer which was formed in dry air [40].

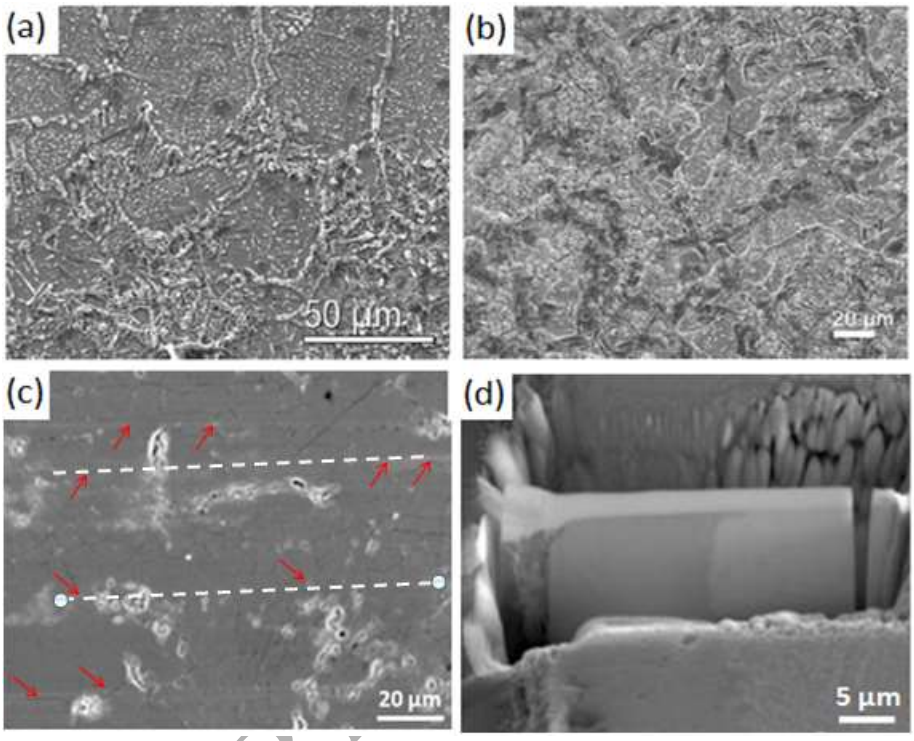

Fig. 13 Surface morphologies of HSS samples oxidised for 30 minutes at temperature of 650 °C (a) in a dry atmosphere [42] and (b) in a humid atmosphere; (c) morphology of a HSS work roll surface in actual service condition after industrial hot rolling process, and (d) FIB image of an ion-milled cross section of practical oxide scale.

In order to understand the influence of oxidation time, two additional HSS samples have been oxidized at 650 °C for 30 minutes in both dry and humid atmospheres, and their surface morphologies are shown in Fig. 13a and b, respectively. It is obvious that increasing oxidation time from 10 minutes to 30 minutes leads to a heavier oxidation of carbides, according to the comparison between Fig. 13 and Fig. 12. TEM observations reveal that the oxide scale consists of two sub-layers under both dry and humid atmospheres. The outer layer is characterized by large oxide crystals, while inner layer has fine oxides and an amount

of pores. Ref. [42] shows more details on the TEM study of oxide scale developed in a dry atmosphere at 650 °C for 30 minutes. Fig. 13c shows morphology of a HSS work roll surface in actual service condition after industrial hot rolling process, and Fig. 13d shows the SEM image of cross section of the practical oxide scale prepared by FIB. The figures reveal that the morphology of practical oxide scale is completely different from those shown in Fig. 11, Fig. 12 and Fig. 13. The shiny HSS work roll surface indicates that the oxide scale is very thin. In fact, careful examination of the oxide scale cross section reveals that the average oxide scale thickness is only about 400 nm. Compared to the oxide scales developed in laboratory, the industrial oxide scale is more compact, which should be attributed to the cyclical mechanical loads (contact stresses) during contacts between the work roll and strip or backup roll. The oxide scales can be deformed by compression and shearing due to existence of the contact stresses, and density of the pores in the oxide scale can be reduced. In Fig. 13c, the bright dashed lines indicate the shearing direction or sliding direction at the industrial HSS work roll surface, which corresponds with the rolling direction. Wear scars at the roll surface have also been observed as marked by red arrows. Mechanical loads also lead to stress localization at the interface between the oxidized carbides and matrix, which leads to formation of micro-cracks or micro-voids. Presence of the micro-voids at work roll surface as shown in Fig. 13c indicates that the oxidation is not uniform and the oxidized carbides are peeled off during hot rolling process. This phenomenon is attributed to the different thermal expansions between the matrix and carbides [53], and the oxidized carbides are subjected to more stress localization when they protrude above the work roll matrix surface during contacts [54]. However, micro-voids have not been observed at the oxide scale surface developed in laboratory. This should be interpreted by less stress localizations in the oxide scales induced by mechanical loads which are not been able to be considered in laboratory oxidation experiment in the present study.

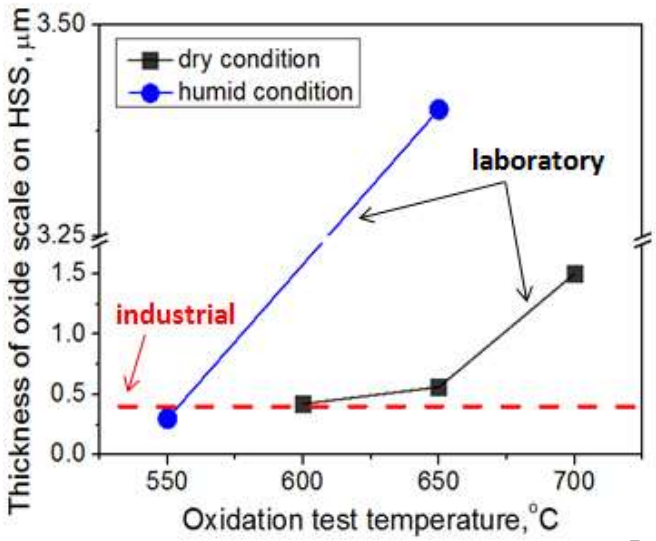

Fig. 14 Comparison of the oxide scale thickness between the oxide scales developed at a HSS work roll surface in actual service condition during industrial hot rolling and in laboratory.

Fig. 14 shows comparison of the oxide scales thickness developed both under practical industry conditions and in laboratory. As can be seen, the oxide scale thickness is significantly influenced by the oxidation atmosphere and temperature. For example, the oxide scale formed in a humid atmosphere at 650 °C is about five times thicker than the one developed in a dry condition. In addition, the oxide scale thickness at 550 °C is smallest and it is less than 300 nm, while the scale thickness at 600 °C is comparable to the industrial one. A slight oxide scale thickness rise can be observed at 650 °C, which can be considered as one of the critical temperatures for this studied HSS material because the figure shows a scale thickness growing rate transition. With further increasing the oxidation temperature up to 700 °C, the scale thickness increases very fast and reaches to about 1.5 μm. In addition to the oxidation temperature and atmosphere, mechanical loads in actual service condition of hot rolling also contributes to the different thicknesses of oxide scales developed in laboratory and industry. According to the reports by Zhou et al. [55] and Xiao et al. [56], stresses are induced in the oxide scale and substrate material during oxidation, and such stresses in return affect the diffusion of ions and vacancy in the oxide layer. Therefore, existence of the mechanical loads leads to the contact stresses, which affect the stress distribution in both oxide scales and substrate and then affect the formation of pores and growth of oxide scales.

It should be noted that more microstructual studies (especially TEM and EBSD) are needed to investigate the defects and crystallographic orientations of those oxide scales developed

in different conditions. As pointed out in the earlier studies [38,46], it is very difficult to study the oxidation behavior in a work roll during industrial hot rolling. The main reasons are: (i) it is not an isothermal condition and it actually comprises part of both the roll bite region and subsequent wiper cooling region where the roll surface temperature is larger than a critical one (oxidation starts); (ii) the oxidation atmosphere is not a simple dry atmosphere or humid atmosphere. The oxidation in the roll bite region can be treated as in a dry condition, but the oxidation in the subsequent wiper cooling region is in a humid condition; and (iii) the influence of mechanical load, thermal stress and initial stress state of the work rolls cannot be neglected. Unfortunately, no experimental or modeling studies able to consider all the above mentioned influencing factors are available now. Therefore, further comprehensive studies on the oxidation mechanism and tribological mechanism of HSS work roll materials in actual service conditions from both the microstructural and theoretical views are still very essential.

7. Conclusion

In this study, the thermal and oxidation behaviours of a HSS work roll during hot rolling in actual service conditions have been systematically investigated, and the following conclusions can be obtained:

(1) Temperature evolution in a HSS work roll of a practical hot strip mill has been systematically studied by an experimentally validated model. The results reveal that the maximum temperature varies from 580 to 650 °C at the roll surface at stand F1 during hot rolling. The maximum surface temperature decreases quickly from stand F1 to F4, and it is only about 340.1°C during one revolution of hot rolling at stand F4.

(2) Thermal stress evolutions during hot rolling and subsequent idling are significantly influenced by the initial work roll body temperature. Magnitude of the maximum compressive circumferential thermal stress decreases obviously from 950 to 750 MPa with increasing the roll body temperature from 25 to 200 °C during hot rolling.

(3) During idling, the HSS work roll surface undergoes pure compression when its initial temperature is 25 °C. By contrast, initial roll temperature of 200 °C leads to a completely tension at the roll surface, which is subjected to both compression and tension at an initial temperature of 100 °C.

(4) The oxidation experiments show that only the carbides but not the steel matrix are slightly oxidized at 550 °C, because of the high free energy at the carbide/matrix

interface and lower thermal stability of the carbides. However, a compact thin oxide scale covers the HSS matrix, and the oxidized carbides protrude above the matrix surface when the oxidation temperature is equal to or larger than 600°C in both dry and humid atmospheres.

(5) The practical HSS oxide scale developed in industry has less thickness than those formed in laboratory, and the surface morphologies are different. Those differences should be attributed to the complicated oxidation atmospheres (not simply dry or humid) at industrial service condition, and influences of the cyclical mechanical load and thermal stress during hot rolling.

Acknowledgements

Dr. Deng would like to acknowledge Australian Academy of Science (AAS) and Japan Society for the Promotion of Science (JSPS) for awarding him an international fellowship. This work was financially supported by the Baosteel-Australia Joint Research and Development Centre (BA12045) and Australian Research Council Discovery Project (DP130103973). Simulations were conducted using the HPC cluster at University of Wollongong and the computing facilities provided by NCI National Facility of Australia.

References

[1] Roberts WL. Hot rolling of steels. Marcel Dekker, New York 1983.

[2] Belzunce FJ, Ziadi A, Rodriguez C. Structural integrity of hot strip mill rolling rolls. Eng Fail Anal 2004;11:789-797.

[3] Garza-Montes-de-Oca NF, Colas R, Rainforth WM. On the damage of a work roll grade high speed steel by thermal cycling. Eng Fail Anal 2011;18:1576-1583.

[4] Deng GY, Zhu Q, Tieu K, Zhu HT, Reid M, Saleh AA, Su LH, Ta TD, Zhang J, Lu C, Wu Q, Sun DL. Evolution of microstructure, temperature and stress in a high speed steel work roll during hot rolling: Experiment and modelling. J Mater Process Technol 2017;240:200-208.

[5] Stevens PG, Ivens KP, Harper P. Increasing work-roll life by improved roll cooling practice. J Iron Steel Inst 1971;209:1-11.

[6] Tseng AA, Tong SX, Maslen SH, Mills JJ. Thermal behaviour of aluminium rolling. J Heat Trans 1990;112:301-308.

[7] Sonboli A, Serajzadeh S. Prediction of thermal stresses and temperature field in work rolls during hot strip rolling process. Mater Sci Technol 2010;26:343-351.

[8] Sonboli A, Serajzadeh S. A model for evaluating thermo-mechanical stresses within work-rolls in hot-strip rolling. J Eng Math 2012;72:73-85.

[9] Deng GY, Lu C, Su LH, Tieu AK, Yu HL, Liu XH. Investigation of sample size effect on the deformation heterogeneity and texture development during equal channel angular pressing. Comp Mater Sci 2013;74:75-85.

[10] Deng GY, Tieu AK, Si LY, Su LH, Lu C, Wang H, Liu M, Zhu HT, Liu XH. Influence of cold rolling reduction on the deformation behaviour and crystallographic orientation development. Comp Mater Sci 2014;81:2-9.

[11] Deng GY, Lu C, Su L, Tieu AK, Li JT, Liu M, Zhu H, Liu X. Influence of outer corner angle on the plastic deformation and texture evolution in equal channel angular pressing. Comp Mater Sci 2014;81:79-88.

[12] Patula EJ. Steady-state temperature distribution in a rotating roll subject to surface heat fluxes and convective cooling. ASME J Heat Transf 1981;103:36-41.

[13] Troeder C, Spielvogel A, Xu JW. Temperature and thermal stresses in work rolls during the hot rolling of strip. Steel Res 1985;56:379-384.

[14] Lai WB, Chen TC, Weng CI. Transient thermal stresses of work roll by coupled thermoelasticity. Comp Mech 1991;9:55-71.

[15] Guo RM. Two-dimensional transient thermal behaviour of work rolls in rolling process. J Manuf Sci Eng 1998;120:28-33.

[16] Hwang SM, Sun CG, Ryoo SR, Kwak WJ. An integrated FE process model for precision analysis of thermo-mechanical behaviours of rolls and strip in hot strip rolling. Comp Methods Appl Mech Eng 2002;191:4015-4033.

[17] Lee JD, Manzari MT, Shen Y, Zeng W. A finite element approach to transient thermal analysis of work rolls in rolling process. Trans ASME J Manuf Sci Eng 2000;122:706-716.

[18] Li CS, Liu XH, Wang GD, He XM. Three-dimensional FEM analysis of work roll temperature field in hot strip rolling. Mater Sci Technol 2002;18:1147-1150.

[19] Li CS, Yu HL, Deng GY, Liu XH, Wang GD. Numerical simulation of temperature field and thermal stress field of work roll during hot strip rolling. J Iron Steel Res Int 2007;14:18-21.

[20] Guerrero MP, Flores CR, Perez A, Colas R. Modelling heat transfer in hot rolling work rolls. J Mater Process Technol 1999;94:52-59

[21] Sun CG, Yun CS, Chung JS, Hwang SM. Investigation of thermomechanical behaviour of a work roll and of roll life in hot strip rolling. Metall Mater Trans A 1998;29:2407-2424.

[22] Chang. Thermal stresses in work rolls during the rolling of metal strip. J Mater Process Technol 1999;94:45-51.

[23] Perez A, Corral RL, Fuentes R, Colas R. Computer simulation of the thermal behaviour of a work roll during hot rolling of steel strip. J Mater Process Technol 2004;153-154:894-899.

[24] Corral RL, Colas R, Perez A. Modeling the thermal and thermoelastic responses of work rolls used for hot rolling steel strip. J Mater Process Technol 2004;153-154:886-893.

[25] Saha JK, Kundu S, Chandra S, Sinha SK, Singhal U, Das AK. Mathematical modelling of roll cooling and roll surface stress. ISIJ Int 2005;45:1641-1650.

[26] Fischer FD, Schreiner WE, Werner EA, Sun CG. The temperature and stress fields developing in rolls during hot rolling. J Mater Process Technol 2004;150:263-269.

[27] Serajzadeh S, Taheri AK, Mucciardi F. Unsteady state work-roll temperature distribution during continuous hot slab rolling. Int J Mech Sci 2002;44:2447-2462.

[28] Serajzadeh S, Mucciardi F. Modelling of work-roll temperature variation at unsteady state condition. Model Simul Mater Sci Eng 2003;11:179-194.

[29] Benasciutti D, Brusa E, Bazzaro G. Finite elements prediction of thermal stresses in work roll of hot rolling mills. Procedia Eng2010;2:707-716.

[30] Na DH, Moon CH, Lee YS. Thermal stress evolution of the roll during rolling and idling in hot strip rolling process. J Therm Stresses 2014;37:981-1001.

[31] Abbaspour M, Saboonchi A. Work roll thermal expansion control in hot strip mill. Appl Math Model 2008;32:2652-2669.

[32] Saboonchi A, Abbaspour M. Changing the geometry of water spray on milling roll and its effect on the work roll temperature. J Mater Process Technol 2004;148:35-49.

[33] Lee ES, Park WJ, Baik KH, Ahn S. Different carbide types and their effect on bend properties of a spray-formed high speed steel. Scripta Mater 1998;39:1133-38.

[34] Kim CK, Kim YC, Park JI, Lee S, Kim NJ, Yang JS. Effects of alloying elements on microstructure, hardness, and fracture toughness of centrifugally cast high-speed steel rolls. Metall Mat Trans A 2005;36:87-97.

[35] Xu L, Wei S, Xing J, Long R. Effects of carbon content and sliding ratio on wear behaviour of high-vanadium high speed steel (HVHSS) under high-stress rolling-sliding contact. Tribology Int 2014;70:34-41.

[36] Xu L, Xing J, Wei S, Zhang Y, Long R. Investigation on wear behaviours of high-vanadium high speed steel compared with high-chromium cast iron under rolling contact condition. Mater Sci Eng A 2006;434:63-70.

[37] Kim HH, Lim JW, Lee JJ. Oxidation behaviour of high speed steels in dry and wet atmospheres. ISIJ Int 2003;43:1983-1988.

[38] Molinari A, Straffelini G, Tomasi A, Biggi A, Corbo G. Influence of microstructure and chromium content on oxidation behaviour of spin cast high speed steels. Mater Sci Tech 2001;17:425-430.

[39] Molinari A, Pellizzari M. Primary carbides in spincast HSS for hot rolls and their effect on the oxidation behaviour. 6th International Tooling Conference 2005:437-452.

[40] Monteiro MJ, Rizzo FC. Effect of chromium content on the oxidation behaviour of high-speed steels under dry and moist air environments. Mater Sci Forum 2005;522-523:171-180.

[41] Zhu Q, Zhu HT, Tieu AK, Reid M, Zhang LC. In-situ investigation of oxidation behaviour in high-speed steel roll material under dry and humid atmospheres. Corros Sci2010;52:2707-2715.

[42] Zhu O, Zhu HT, Tieu AK, Kong C. Three dimensional microstructure study of oxide scale formed on a high-speed steel by means of SEM, FIB and TEM. Corros Sci 2011;53:3603-3611.

[43] Zhou L, Liu F, Liu CS, Sun DL. High temperature oxidation behaviour of high speed steel for roll in water vapour, Trans Mater Heat Treat 2004;25:134-138.

[44] Zhou L, Liu F, Liu CS, Sun DL. High temperature oxidation behaviour of high speed steel for hot rolling rollers. J Iron Steel Res 2005;17:60-63.

[45] Garza-Montes-de-Oca NF, Colas R, Rainforth WM. High temperature oxidation of a work roll grade high speed steel. Oxid Met 2011;76:451-468.

[46] Yin Y, Sun J, Teng S, Niu C. Oxidation behaviour of high-speed steel used for hot rolls. Oxid Met 2016;86:45-57.

[47] Colas R. Modelling heat transfer during hot rolling of steel strip. Modelling Simul Mater Sci Eng1995;3:437-453.

[48]Ginzburg VB. Application of coolflex model for analysis of work roll thermal condition in hot strip mills. Iron and Steel Engineer 1997;11:38-45.

[49] Abaqus theory manual (version 6.11-1) 2011.

[50] Song XY, Zhang XJ, Fu LC, Yang HB, Yang K, Zhu L. Evaluation of microstructure and mechanical properties of 50Cr5NiMoV steel for forged backup roll. Mater Sci Eng A 2016;677:465-473.

[51] Qin XF, Sun DL, Xie LY, Wu Q. Hardening mechanism of Cr5 backup roll material induced by rolling contact fatigue. Mater Sci Eng A 2014;600:195-199.

[52] Saunders SRJ, Monteiro M, Rizzo F. The oxidation behaviour of metals and alloys at high temperatures in atmospheres containing water vapour: A review. Prog Mater Sci 2008;53:775-837.

[53] Vergne C, Boher C, Gras R, Levaillant C. Influence of oxides on friction in hot rolling: Experimental investigations and tribological modelling. Wear 2006;260:957-975.

[54] Joos O, Boher C, Vergne C, Gaspard C, Nylen T, Rezai-Aria F. Assessment of oxide scales influence on wear damage of HSM work rolls. Wear 2007;263:198-206.

[55] Zhou H, Qu J, Cherkaoui M. Stress-oxidation interaction in selective oxidation of Cr-Fe alloys. Mech Mater 2010;42:63-71.

[56] Xiao J, Prud'homme N, Li N, Ji V. Influence of humidity on high temperature oxidation of Inconel 600 alloy: Oxide layers and residual stress study. Appl Surf Sci 2013;284:446-452.

Graphical abstract: